Macromolecules

pubs.acs.org/Macromolecules Article

Dual Origin of Viscoelasticity in Polymer-Carbon Black Hydrogels: A Rheometry and Electrical Spectroscopy Study

Gauthier Legrand, Sébastien Manneville, Gareth H. McKinley, and Thibaut Divoux*

Cite This: *Macromolecules* 2023, 56, 2298−2308 Read Online

ACCESS | Metrics & More | Article Recommendations | Supporting Information

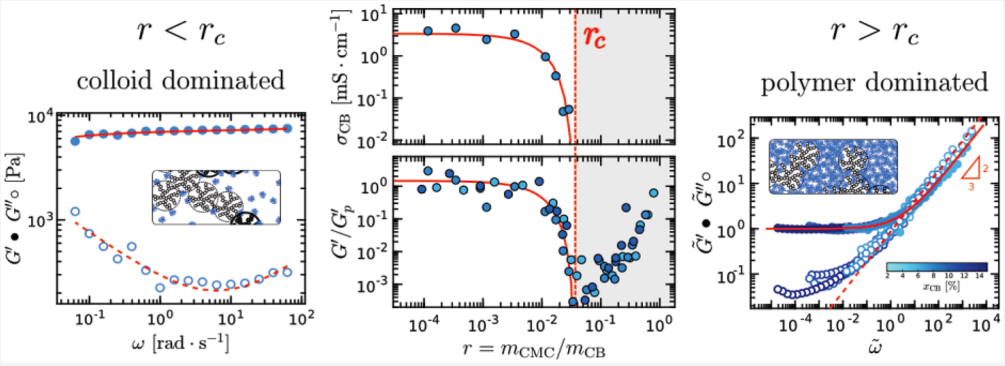

ABSTRACT: Nanocomposite gels formed by mixing nanoparticles and polymers offer a limitless creative space for the design of functional advanced materials with a broad range of applications in materials and biological sciences. Here, we focus on aqueous dispersions of hydrophobic colloidal soot particles, namely, carbon black (CB) dispersed with a sodium salt of carboxymethylcellulose (CMC), a food additive known as cellulose gum that bears hydrophobic groups, which are liable to bind physically to CB particles. Varying the relative content of CB particles and cellulose gum allows us to explore a rich phase diagram that includes a gel phase observed for a large enough CB content. We investigate this hydrogel using rheometry and electrochemical impedance spectroscopy. CB−CMC hydrogels display two radically different types of mechanical behaviors that are separated by a critical CMC-to-CB mass ratio r_c. For $r < r_c$, i.e., for low CMC concentration, the gel is electrically conductive and shows a glassy-like viscoelastic spectrum, pointing to a microstructure composed of a percolated network of CB particles decorated by CMC. In contrast, gels with a CMC concentration larger than r_c are nonconductive, indicating that the CB particles are dispersed in the cellulose gum matrix as isolated clusters, and act as physical cross-linkers of the CMC network, hence providing mechanical rigidity but limited conductivity enhancement to the composite. Moreover, in the $r > r_c$ concentration range, CB−CMC gels display a power-law viscoelastic spectrum that depends strongly on the CMC concentration. These relaxation spectra can be rescaled onto a master curve, which exhibits a power-law scaling in the high-frequency limit, with an exponent that follows Zimm theory, showing that CMC plays a key role in the gel viscoelastic properties for $r > r_c$. Our results offer an extensive experimental characterization of CB−CMC dispersions that will be useful for designing soft nanocomposite gels based on hydrophobic interactions.

INTRODUCTION

Carbon black (CB) particles are colloidal soot particles produced from the incomplete combustion of fossil fuels. These textured particles of typical size 0.5 μm are made of permanently fused "primary" nanoparticles of diameter 20−40 nm.[1] Cheap and industrially produced at large scale, they are broadly employed for their mechanical strength, high surface area, and their electrical conductive properties, even at low volume fractions. Applications include pigments for ink,[2,3] reinforcing fillers in tires and other rubber products,[4,5] electrically conductive admixture in cement,[6] conductive materials for supercapacitors,[7] biosensors,[8−10] and electrodes for semisolid flow batteries.[11−15] Being much cheaper than carbon nanotubes or graphene, CB particles appear promising for applications in energy storage,[16] including flow electrodes for which the ultimate goal is to maximize the conductivity, while minimizing the shear viscosity of the material. In that framework, flow batteries based on aqueous dispersion of carbon black nanoparticles have recently received an upsurge of interest.[12,17−20]

Due to their hydrophobic properties, CB particles are easily dispersed in aprotic solvents such as hydrocarbons,[21] where

Received: October 7, 2022
Revised: February 14, 2023
Published: March 14, 2023

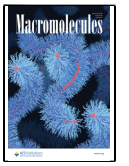

https://doi.org/10.1021/acs.macromol.2c02068
Macromolecules 2023, 56, 2298−2308

particles interact only via van der Waals forces[22] that correspond to a short-range attractive potential, whose depth is typically about 30 k_BT in light mineral oil.[23] As a result, CB dispersions organize into space-spanning networks even at low volume fractions and behave as soft gels[24−26] characterized by a yield stress at rest and a highly time-dependent mechanical response under external shear, which involves delayed yielding, heterogeneous flows,[27−30] and shear-induced memory effects.[31−33]

In contrast, untreated CB particles are difficult to disperse in water where they tend to flocculate rapidly, before creaming or sedimenting.[18,34] Stabilizing aqueous dispersions of CB particles requires keeping the particles apart, either by electrostatic repulsion or by steric hindrance. In practice, this is achieved in three different ways: (i) surface oxidation yielding acidic functional groups,[35] (ii) functionalization of CB particles with polymers, i.e., polymer grafting chemically onto their surface[36−42] or CB encapsulation through emulsion polymerization,[43,44] and (iii) physical adsorption of a polymer dispersant. The latter method allows CB mass fractions in water to be as large as 20%, and the dispersants investigated include polyelectrolytes,[45] ionic surfactants,[46,47] such as sulfonate surfactants,[48−51] sulfonic acids,[52,53] cetyltrimethylammonium bromide (CTAB),[50,54−57] and chloride (CTAC),[58] and nonionic surfactants,[50,59] such as silicone surfactants[60] or block copolymers surfactants,[59,61,62] as well as biopolymers, such as Arabic gum[18,63] or polysaccharides.[64−67] From a structural point of view, dispersants adsorb as monolayers onto the surface of CB particles due to hydrophobic interactions, whose strength depends on the molecular structure and weight of the dispersant.[51,66] Irrespective of the nature of the dispersant, such stabilized CB dispersions behave as shear-thinning fluids.[65,67,68] However, depending on the formulation, CB−polymer mixtures may present a solid-like behavior at rest with weakly time-dependent properties,[53,62,66] suggesting the presence of a percolated network of the CB particles.[69]

The large variety of dispersants used so far in CB dispersions is in stark contrast with the limited knowledge regarding the link between the microstructure and rheological properties of the resulting composite materials. Among the open questions, it remains to disentangle the respective contributions of the CB and the dispersant to the macroscopic mechanical properties of the mixture and to investigate whether the CB particles form a percolated network on their own or if they are bridged by the polymeric chains.

Here, we perform such an in-depth study with a semiflexible anionic polysaccharide dispersant, namely, carboxymethylcellulose (CMC). CMC is a water-soluble cellulose ether, which is commonly used as a water binder and thickener in pharmacy, cosmetics, and food products[70] and as a dispersing agent in semisolid flow batteries,[65] while showing a great potential for biomedical applications.[71] The solubility and overall properties of CMC are set primarily by its molecular weight and to a lesser extent by its degree of substitution (DS).[72,73] The latter is defined as the number of hydrogen atoms in hydroxyl groups of glucose units replaced by carboxymethyl and varies typically between 0.4 and 1.2 with up to a maximum value of 3.[70] Over a broad range of concentrations, CMC aqueous solutions are shear-thinning viscoelastic liquids.[74,75] However, weakly substituted CMCs, i.e., with DS values lower than about 1, display hydrophobic interactions that favor interchain association in aqueous solution, yielding larger viscosities and eventually leading to a sol−gel transition for large enough polymer concentrations.[76−81]

In the present work, we take advantage of such hydrophobic regions on CMC molecules to use this polymer as a dispersant of CB particles. Varying the contents of CB and CMC, we unravel a rich phase diagram, which we characterize by rheometry and electrochemical impedance spectroscopy. The outline of the manuscript is as follows: after presenting the materials and methods, we introduce the phase diagram and focus specifically on the hydrogel phase. We then discuss the impact of the CMC concentration on the gel elastic properties before turning to the role of the CB content. Our results allow us to identify two different types of hydrogels, whose microstructures are sketched and extensively discussed before concluding.

MATERIALS AND METHODS

Samples are prepared by first dissolving sodium carboxymethyl cellulose (Sigma-Aldrich, M_w = 250 kg mol^{-1} and DS = 0.9) in deionized water. Stock solutions up to 5% wt. are prepared and stirred at room temperature for 48 h until homogeneous, before adding the CB particles (VXC72R, Cabot). Samples are placed in a sonicator bath for two rounds of 90 min separated by a period of 24 h under mechanical stirring. The samples are finally left at rest for another 24 h before being tested. The CMC solution is considered to be the solvent, while CB particles are the dispersed phase; hence, we define the CMC weight concentration as $c_{CMC} = m_{CMC}/(m_{CMC} + m_{water})$ and the CB weight fraction as $x_{CB} = m_{CB}/(m_{CB} + m_{CMC} + m_{water})$, where m_{CB}, m_{CMC}, and m_{water} are, respectively, the mass of CB, CMC, and water in the sample.

Rheological measurements are performed with a stress-controlled rheometer (MCR 302, Anton Paar) equipped with a cone-and-plate geometry (angle 2°, radius 20 mm). For very soft samples with elastic moduli lower than 10 Pa, we use a larger cone-and-plate geometry (angle 2°, radius 25 mm), whereas for the stiffest samples with elastic moduli larger than 10 kPa, we use a parallel-plate geometry (gap 1 mm, radius 20 mm). For all the geometries used, the stator is smooth and the rotor is sandblasted. Finally, to ensure a reproducible initial state following the loading step into the shear cell of the rheometer, each sample is shear-rejuvenated at $\dot{\gamma}$ = 500 s^{-1} (or $\dot{\gamma}$ = 50 s^{-1} for samples with elastic moduli larger than 10 kPa), before being left at rest for 1200 s, during which we monitor the linear viscoelastic properties through small amplitude oscillatory shear (γ_0 = 0.03−0.3% and f = 1 Hz; see Figure S1).

Electrical measurements are performed in AC mode in a cylindrical cell made of Teflon (thickness of about 1 mm and surface of about 0.5 cm^2). The inner sides are made of metal and act as electrodes that are connected to a multifrequency impedance analyzer (SP-300 Potentiostat, Biologic). A decreasing ramp of frequency allows one to determine the frequency dependence of the sample impedance $Z^*(f) = Z' - iZ''$; the real and imaginary parts, Z' and Z'', respectively, are shown in Figure 1 for a sample containing c_{CMC} = 0.15% wt. and x_{CB} = 8% wt. The resistance Z' shows a decreasing step shape, while the reactance Z'' displays a bell-shaped curve. Overall, the complex impedance measured experimentally can be well fitted by

$$Z^*(f) = R_{CB}\frac{1 + R_{ion}Q(i2\pi f)^n}{1 + (R_{CB} + R_{ion})Q(i2\pi f)^n} \quad (1)$$

which corresponds to the simple circuit sketched as an inset in Figure 1 and classically reported in the literature for describing the electrical response of CB or carbon nanotube dispersions.[13,19,33,82,83] Equation 1 accounts for the additive contributions of the ions in solution and an electronically conductive percolated network of CB particles. More precisely, the circuit comprises a resistance R_{CB} modeling the percolated network of CB particles, in parallel with two elements, namely, a resistance R_{ion} accounting for the ionic conductivity of the

https://doi.org/10.1021/acs.macromol.2c02068
Macromolecules 2023, 56, 2298−2308

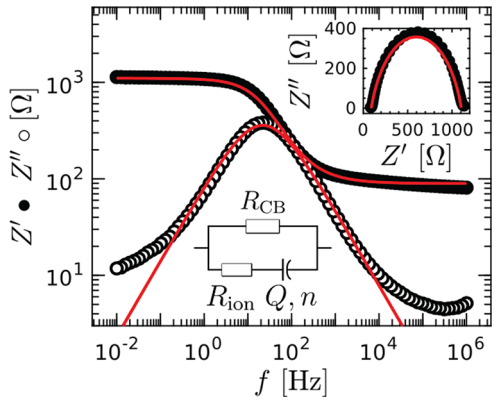

Figure 1. Frequency dependence of the resistance Z' (●) and reactance Z'' (○) of a CMC−CB dispersion. Inset: Nyquist plot Z'' vs Z' for the same data. Measurement performed in AC mode by ramping down the frequency from $f = 10^6$ to 10^{-2} Hz. Each point is averaged over two cycles. The red continuous curves in both the main graph and the inset show the best fit of the data for Z' and Z'' simultaneously by eq 1, which corresponds to the electrical circuit sketched in the main graph with $R_{ion} = 97$ Ω, $R_{CB} = 1.1$ kΩ, $n = 0.78$, and $Q = 1.8 \times 10^{-5}$ $\Omega^{-1}\cdot s^n$. Data obtained on a sample composed of $c_{CMC} = 0.15\%$ wt. and $x_{CB} = 8\%$ wt.

sample in series with a constant phase element (CPE) characterized by a dimensionless exponent n and a parameter Q. CPEs were first introduced in the context of particulate suspensions[84] and model the electrode−electrolyte interface as an imperfect capacitor.[85,86] Although such modeling fails to describe the dependence of $Z''(f)$ at very low and very high frequencies, potentially due to some parasitic inductance, it does account very well for $Z'(f)$ over 8 orders of magnitude in frequency. Fitting the impedance spectra to eq 1 yields four parameters, R_{CB}, R_{ion}, Q, and n. The two resistances can be converted into electrical conductivities $\sigma_{CB} = k/R_{CB}$ and $\sigma_{ion} = k/R_{ion}$, k being the cell constant determined by independent measurements on KCl solutions of different concentrations (here $k = 0.37 \pm 0.01$ cm^{-1}; see Figure S2). The parameters Q and n are weakly sensitive to the CB and CMC content, and their typical values are $Q \simeq 17 \times 10^{-6}$ $\Omega^{-1}\cdot s^n$ and $n \simeq 0.75$, as discussed in more detail in the Supporting Information (see Figure S3). In the rest of the manuscript, we focus on σ_{CB}, which is used as a proxy for probing the existence of a space-spanning percolated network of CB particles in the sample and, therefore, provides some insights on the microstructure of the CB−CMC dispersions.

RESULTS AND DISCUSSION

Phase Diagram. We first discuss qualitatively the outcome of dispersing carbon black (CB) nanoparticles in a solution of carboxymethylcellulose (CMC). In practice, we observe four different phases that are summarized in the phase diagram reported in Figure 2. We emphasize that such a phase diagram of the polymer/carbon mixture is a *nonequilibrium* state diagram whose boundaries depend on the details of the sample preparation. For low CB and CMC concentration, the aqueous dispersion is unstable and the CB particles sediment within about 20 min [Figure 2b]. On the one hand, increasing the CMC concentration beyond about 10^{-2}% allows stabilization of the CB particles, yielding a viscoelastic liquid being stable over weeks [Figure 2c]. On the other hand, increasing the content in CB particles confers gel-like properties upon the samples; i.e., the sample shows a solid-like behavior at rest and for small deformations, while it flows for large enough stresses [Figure 2d]. Finally, for CB content larger than about 10% wt., the sample behaves as a strongly elastic paste, with a fragile behavior to the touch [Figure 2e].

In the present work, we focus on the hydrogel phase, which is observed over the entire range of CMC concentrations explored and for CB content ranging between a few % wt. and about 15% wt. In order to quantify the gel rheological properties, we measure its linear viscoelastic properties through small amplitude oscillatory shear, as detailed above. The ratio of the viscous to the elastic modulus measured at $\omega = 2\pi$ rad·s^{-1}, i.e., $G''/G' = \tan\delta$, also known as the loss factor, is reported in Figure 3 (see Figures S4 and S5 for a similar representation of G' and G'', respectively). Such a phase diagram built upon the loss factor highlights two different regions, which correspond to samples that mainly differ by their CMC concentration. Samples with a lower CMC concentration display relatively less viscous dissipation ($\tan\delta \lesssim 0.1$) than samples with the highest CMC concentration ($\tan\delta \gtrsim 0.1$). This observation suggests that CMC−CB hydrogels come in two different flavors, depending on the polymer content. We quantify these qualitative results by studying the scaling of the viscoelastic and electrical properties of the samples, with respect to the CMC concentration and the CB content.

Impact of CMC Concentration on the Gel Elastic Properties. In this section, we first discuss the impact of the CMC concentration at fixed CB content, which corresponds to

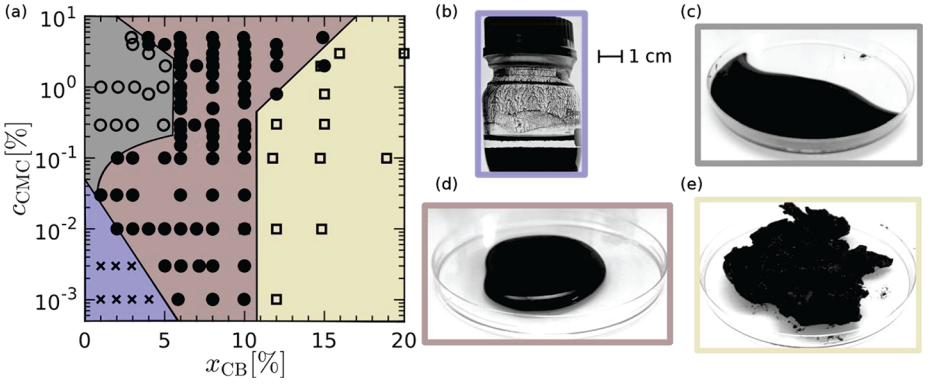

Figure 2. (a) Phase diagram of aqueous CMC−CB dispersions as a function of the CB solid weight fraction x_{CB} and the CMC weight fraction c_{CMC}. Pictures of (b) demixed phase [blue region and × symbols in (a)], (c) the viscoelastic liquid phase [gray region and ○ symbols in (a)], (d) the viscoelastic solid phase [red region and ● symbols in (a)], and (e) the brittle paste phase [yellow region and □ symbols in (a)].

https://doi.org/10.1021/acs.macromol.2c02068
Macromolecules 2023, 56, 2298−2308

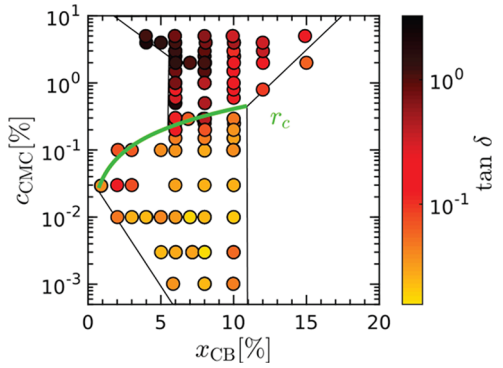

Figure 3. Hydrogel region of the phase diagram of aqueous CMC−CB dispersions as a function of the CB solid weight fraction x_{CB} and the CMC weight fraction c_{CMC}. Color levels code for the loss factor $\tan\delta = G''/G'$ of the gel phase determined by small amplitude oscillatory shear at $\omega = 2\pi$ rad·s^{-1}. The green curve corresponds to $r = r_c$ and separates two regions in the gel phase with samples of different microstructures.

a vertical cut in the phase diagram reported in Figure 2a. The dependence of G' with the CMC concentration is pictured in Figure 4a, as a function of the mass ratio $r = m_{CMC}/m_{CB} = c_{CMC}(1 - x_{CB})/x_{CB}$, which represents the effective number of CMC molecules per CB particles. At low CMC concentrations, we observe that the elastic modulus G' is constant $G' = G'_p$, independent of r over about two decades of CMC concentration, i.e., $10^{-4} \leqslant r \leqslant 10^{-2}$. For $r > 10^{-2}$, the elastic modulus drops abruptly by about 3 orders of magnitude for increasing CMC concentration within a narrow range of r values, reaching a minimum value at $r = r_c \simeq 0.037$. Finally, for $r > r_c$, increasing the CMC concentration translates into an increase of G', which scales roughly as a power-law function of r. This evolution of G' over the whole range of r is robust, as evidenced by the data reported in Figure 4a for three different CB contents, namely, x_{CB} = 6%, 8%, and 10%, as emphasized in Figure S6.

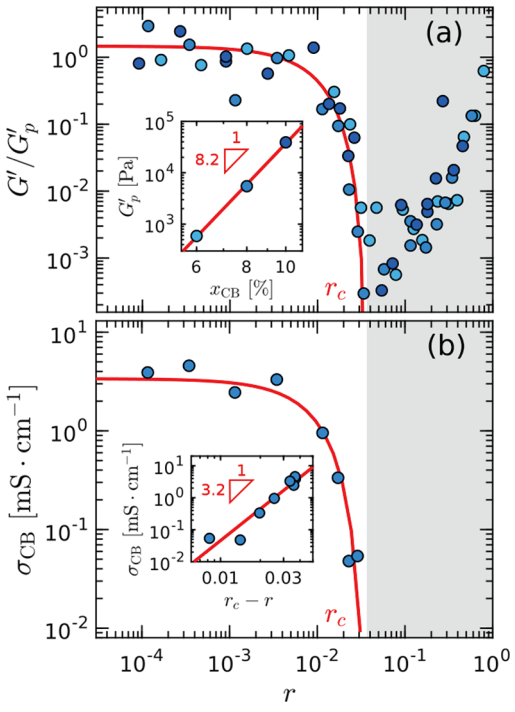

Figure 4. Evidence for a transition between two rheological and electrical regimes. (a) Normalized elastic modulus G'/G'_p measured at $\omega = 2\pi$ rad·s^{-1} vs mass ratio $r = m_{CMC}/m_{CB}$. Each data point has been measured 1200 s after a shear rejuvenation step (see "Materials and Methods"). Color encodes the CB content x_{CB}: 6% (light blue ●), 8% (medium blue ●), and 10% (dark blue ●). The plateau elastic modulus G'_p is defined as the average value of G' over the range $10^{-4} \leqslant r \leqslant 10^{-2}$. The red curve is the best power-law fit of G'/G'_p vs $r_c - r$ with $r_c = 0.037$, yielding an exponent 3.8 ± 0.5. Inset: G'_p vs x_{CB}. The red line is the best power-law fit of the data, yielding an exponent 8.2 ± 0.6. Inset: G'_p vs x_{CB}. (b) Electrical conductivity σ_{CB} of the CMC−CB dispersions vs mass ratio $r = m_{CMC}/m_{CB}$, with x_{CB} = 8% wt. The red curve is the best power-law fit of σ_{CB} vs $(r_c - r)$ with $r_c = 0.037$, yielding an exponent 3.2 ± 0.8. (See inset for a logarithmic plot).

These observations unambiguously confirm the trends determined thanks to the loss factor and show that the linear elastic properties of the CMC−CB hydrogels have two distinct origins depending on the relative content in CB and CMC. For $r < r_c$, the gel elastic properties are set by the amount of CB particles [see inset in Figure 4a] and independent of the CMC concentration, whereas for $r > r_c$, the elastic modulus is an increasing function of the CMC concentration, irrespective of the CB content. Moreover, these results suggest that the gel microstructure is drastically different on each side of r_c. To get more insights on the hydrogel microstructure, we build upon the fact that the CB particles are electrically conductive.

We have performed AC electrical measurements on a series of gels with a fixed CB content (x_{CB} = 8% wt.) and over a broad range of CMC concentrations. For each gel, we determine its electrical conductivity σ_{CB}, associated with the possible percolated network of CB particles (see Materials and Methods for details about electrical measurements). The data are reported in Figure 4b. We observe that the electrical conductivity shows a similar dependence upon the CMC concentration to that of the elastic modulus. For $r < r_c$, the electric conductivity is high, i.e., $\sigma_{CB} \simeq 10$ mS·cm^{-1}, independent of the CMC concentration, whereas for $r > r_c$, the electric conductivity drops by 3 orders of magnitude down to a negligible value following a power law of $r_c - r$, with an exponent 3.2 [see inset in Figure 4b].

These results demonstrate that CB particles form a space-spanning network for $r < r_c$, turning the sample into an electrically conductive material. In contrast, the negligible electrical conductivity ($\sigma_{CB} \lesssim 10^{-3}$ mS·cm^{-1}) observed for $r > r_c$ points toward a microstructure in which the CB particles are isolated as individual particles or clusters. We can further conclude that these isolated particles or clusters serve as a physical cross-linker, which provide solid-like properties to the CMC matrix, for CMC dispersions alone behave as viscoelastic liquids regardless of the CMC concentration.[74,75] These two different microstructures are sketched in Figure 5. Finally, note that the transition from a gel network in which the elasticity is set by the CB particles alone to a gel network in which the elasticity results from the polymer network physically cross-linked by CB particles occurs over a narrow range of r values. The value $r_c \simeq 0.037$ corresponds to the critical amount of polymer required to decorate all the CB particles, such that further addition of CMC only viscosifies the solvent. Within this framework, the evolution of the sample microstructure from $r < r_c$ to $r > r_c$ is akin to a depercolation transition, as reported in silica−styrene−butadiene nanocomposites.[87]

Having identified two different microstructures on each side of r_c, we now determine in detail their respective linear

https://doi.org/10.1021/acs.macromol.2c02068
Macromolecules 2023, 56, 2298−2308

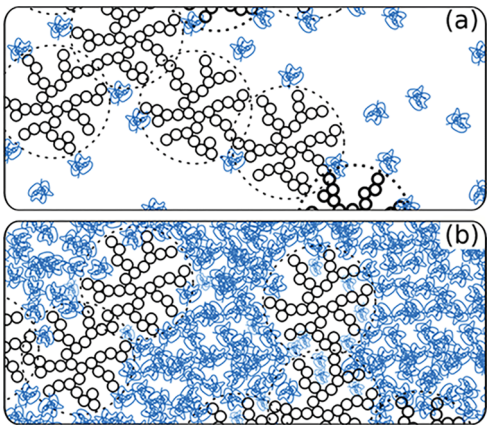

Figure 5. Sketch of CMC−CB hydrogel microstructure in (a) the colloid-dominated regime $r < r_c$ and (b) the polymer-dominated regime $r > r_c$. The black solid circles represent the primary CB nodules, which form the unbreakable fractal CB particles that are individually identified by dashed circles, while the blue coils represent CMC molecules.

viscoelastic properties, namely, their linear viscoelastic spectrum and the impact of the CB content.

Polymer-Dominated Regime ($r > r_c$). We first report on the properties of gels obtained for $r > r_c$, whose microstructure is a viscoelastic matrix of CMC, physically cross-linked by CB particles dispersed individually or as clusters [see Figure 5b].

We first characterize the gel linear viscoelastic properties by determining its viscoelastic spectrum over three decades of frequencies ω. Figure 6a−c shows the viscoelastic spectrum for x_{CB} = 6, 8, and 10% wt. at a fixed CMC concentration c_{CMC} = 2%. These three viscoelastic spectra all display a finite plateau modulus in the zero frequency limit, confirming that these mixtures behave as soft solids at rest. Moreover, for these three spectra, $G''(\omega)$ displays a power-law dependence, at least over two decades in frequency. Both behaviors are well captured by a *fractional* Kelvin−Voigt model, which consists of a spring of stiffness G_0 in parallel with a spring-pot element[88,89] characterized by a quasi-property $\mathbb{V}$ (dimension Pa·s$^{\alpha}$) and an exponent $0 < \alpha < 1$ [see inset in Figure 6a for a sketch of the mechanical model]. Such a fractional element, which was first introduced by Scott-Blair[90] to describe the power-law spectrum of protein gels, plays the same role as the CPE element used to describe the impedance spectra and gives rise to a constant mechanical phase with $\tan\delta = \alpha\pi/2$. The fractional Kelvin−Voigt model yields the following expression for the complex modulus:

$$G^* = G_0 + \mathbb{V}(i\omega)^{\alpha} \tag{2}$$

whose real and imaginary parts correspond to the red fits in Figure 6a−c determined simultaneously. This fit function relies only on two dimensional parameters, namely, the elastic modulus G_0 and the characteristic frequency defined as $\omega_0 = (G_0/\mathbb{V})^{1/\alpha}$. Remarkably, all spectra obtained by varying the carbon content between 6 and 15% wt. at fixed c_{CMC} = 2% can be described by varying G_0 and $\mathbb{V}$, while fixing $\alpha = 2/3$.

Such a robust description allows us to propose a universal master curve for the viscoelastic spectrum obtained at various CB contents, by using the following set of normalized coordinates: $\tilde{G}' = G'/G_0$, $\tilde{G}'' = G''/G_0$, and $\tilde{\omega} = \omega/\omega_0$ [Figure 6d]. This master curve is, in turn, well described over 8 orders of magnitude of reduced frequency by the fractional Kelvin−Voigt model pictured as red lines in Figure 6d. The power-law dependence of both $\tilde{G}'$ and $\tilde{G}''$ with an exponent 2/3 in the high-frequency limit is in remarkable agreement with the value computed by Zimm for dense polymer suspensions and polymer solids taking into account Brownian motion and hydrodynamic interactions.[91,92] This observation strongly suggests that CB particles contribute mainly to the low-frequency part ($\tilde{\omega} \ll 1$) of the viscoelastic spectrum, whereas the CMC entangled network dominates the

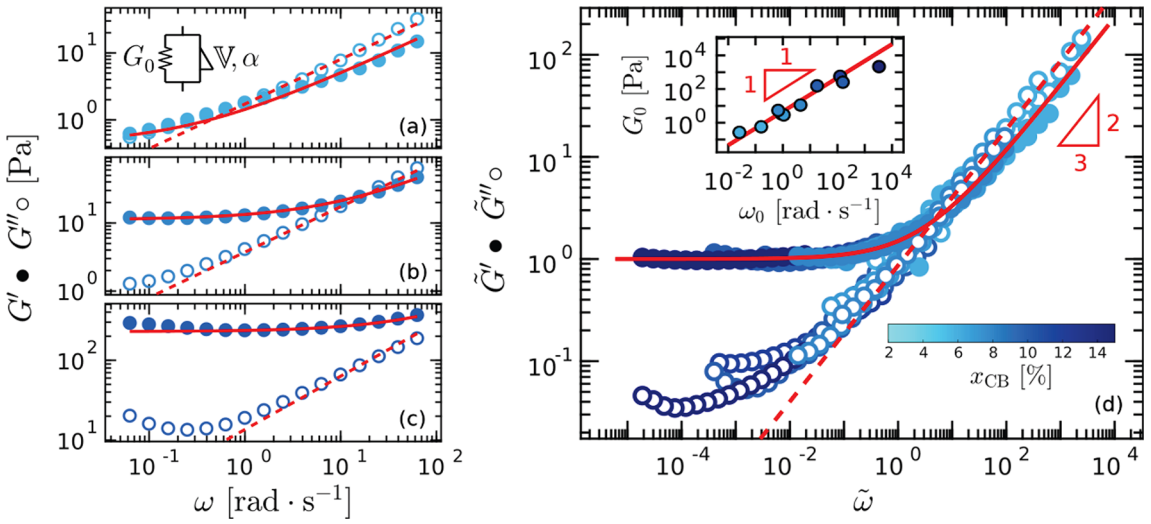

Figure 6. Viscoelastic spectrum in the polymer-dominated regime. Frequency dependence of the elastic and viscous moduli, G' and G'' respectively, of CMC−CB dispersions with three different CB contents x_{CB} = (a) 6%, (b) 8%, and (c) 10% with c_{CMC} = 2%. The red curves are the best fits of the data to a fractional Kelvin−Voigt (FKV) model [see eq 2], which is sketched in (a). (d) Master curve for the frequency dependence of the viscoelastic moduli of CMC−CB dispersions, obtained by normalizing both the moduli and the frequency: $\tilde{G}' = G'/G_0$, $\tilde{G}'' = G''/G_0$, and $\tilde{\omega} = \omega/\omega_0$ with $\omega_0 = (G_0/\mathbb{V})^{1/\alpha}$ for different CB contents ranging from 6% to 15% with c_{CMC} = 2%. The red curves correspond to the normalized FKV model $\tilde{G}^* = 1 + (i\tilde{\omega})^{\alpha}$ with $\alpha = 2/3$. Inset: G_0 vs ω_0; the red continuous line is the best linear fit of the data.

https://doi.org/10.1021/acs.macromol.2c02068
Macromolecules 2023, 56, 2298−2308

high-frequency response ($\tilde{\omega} \gg 1$). This result, together with the fact that CB−CMC hydrogels are not electrically conductive for $r > r_c$, provides robust evidence that, in the regime $r > r_c$, the gel microstructure consists of a CMC viscoelastic matrix in which CB particles are dispersed without forming a percolated network, while serving as cross-linkers. Finally, note that the master curve is robust and holds for different CMC concentrations, as illustrated in Figure S7.

We now discuss the dependence of the plateau modulus G_0 that characterizes the gel elasticity as a function of both the CB content and the CMC concentration. As reported in Figure 7,

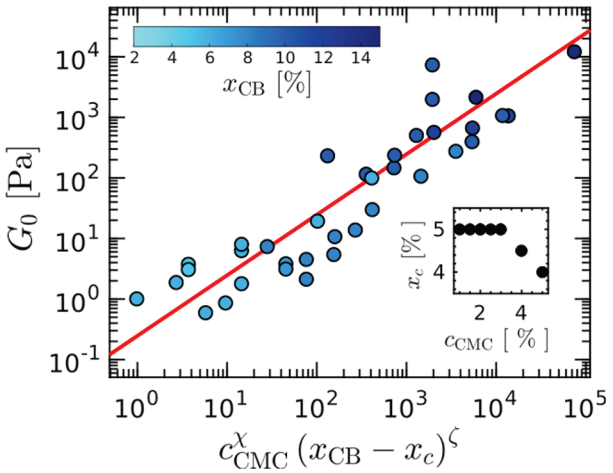

Figure 7. Scaling of the elastic modulus in the polymer-dominated regime. G_0 vs $c_{CMC}^{\chi}(x_{CB} - x_c)^{\zeta}$ for $r > r_c$, where $\chi = 2.4 \pm 0.4$ and $\zeta = 3.0 \pm 0.5$. The inset shows the threshold of CB content x_c as a function of c_{CMC} inferred from the sol−gel transition in the phase diagram reported in Figure 2. The red line shows the best linear fit of the data.

all our experimental results collapse on a master curve when G_0 is plotted as a function of $c_{CMC}^{\chi}(x_{CB} - x_c)^{\zeta}$. On the one hand, the gel elasticity increases as a power law of the particle content relative to the mechanical percolation threshold x_c, which depends on the CMC concentration (see inset in Figure 7) and was determined from the phase diagram in Figure 2. In practice, the onset of rigidity decreases weakly for increasing polymer concentration, from $x_c = 5\%$ at $c_{CMC} = 1\%$ to $x_c = 4\%$ at $c_{CMC} = 5\%$. On the other hand, the gel elasticity increases as a power law of the CMC concentration, with an exponent $\chi = 2.4$. This scaling is strongly reminiscent of the concentration dependence predicted for the plateau modulus of entangled polymer solutions, for which an exponent $7/3 \simeq 2.33$ was derived by Colby, Rubinstein, and Viovy.[93] In the present case, for $r > r_c$, CMCs are indeed in an entangled regime, which is reported[94] for $c_{CMC} \gtrsim 0.16\%$ wt. This result further supports the idea that, for $r > r_c$, the elasticity of the CMC−CB hydrogel has two independent physical origins: a first contribution from the entangled CMC and a second one from the CB particles, which serve as cross-linkers and inhibit the long-time relaxation of the CMC matrix, leading to solid-like behavior at rest.

Colloid-Dominated Regime ($r < r_c$). Let us now consider the case $r < r_c$, where the CMC−CB hydrogel microstructure is formed by a space-spanning network of CB particles decorated with CMC polymers [see Figure 5a]. The viscoelastic spectra of two representative gels containing $c_{CMC} = 10^{-2}\%$ and $x_{CB} = 6$ and 8% wt., respectively, are illustrated in Figure 8a,b. For both gels, G' is merely frequency independent, whereas G'' decreases with increasing frequency and shows a flattening or even a slight upturn in the high-frequency limit [see Figure 8a], which is the signature of the solvent viscosity and Brownian motion of the CB particles.[95] Such a frequency spectrum, along with the logarithmic aging dynamics reported in Figure S1a−c, shows that CMC−CB hydrogels display a glassy-like behavior for $r < r_c$, similar to that reported for jammed assemblies of soft particles[96] or fractal colloidal gels.[97,98] Therefore, we fit the viscoelastic spectrum reported in Figure 8a,b using a modified version of the Soft Glassy Rheology (SGR) model, which is well-known to capture such a behavior and reads:[99−102]

$$G' = \mathcal{G}_0(1 - (\omega\tau)^{x-1}) + c\omega^{1/2} \tag{3}$$

$$G'' = \mathcal{G}_0(\omega\tau)^{x-1} + c\omega^{1/2} + \eta_\infty\omega \tag{4}$$

where x corresponds to a mean-field noise temperature, τ denotes the effective sample age, and the terms $c\omega^{1/2}$ and $\eta_\infty\omega$ account, respectively, for Brownian motion and for the solvent viscous contribution.[103] The data are fitted using eqs 3 and 4 with $\mathcal{G}_0$, x, and c as free parameters. The parameter $\tau = 1200$ s is the time elapsed since the end of the rejuvenation step and $\eta_\infty = 2 \times 10^{-3}$ Pa·s is the viscosity of the CMC solution at $c_{CMC} = 0.01\%$, measured independently with an Ubbelholde viscosimeter. Fitting our experimental data for samples prepared with a CB content ranging between 2% and 12%

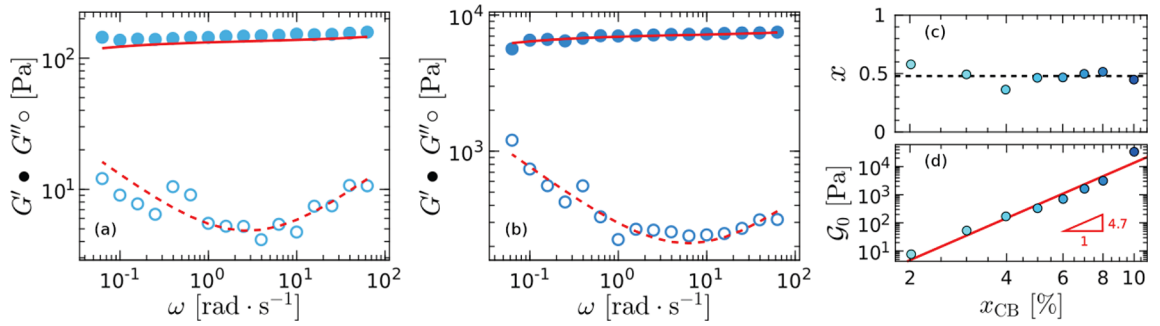

Figure 8. Viscoelastic spectrum in the colloid-dominated regime. Frequency dependence of the elastic and viscous moduli, G' and G'', respectively, of CMC−CB hydrogels with two different CB contents (a) $x_{CB} = 6\%$ and (b) 8% wt. and a fixed amount of CMC polymer, i.e., $c_{CMC} = 0.01\%$ wt. The red curves are the best fits of the data to a modified SGR model [see eqs 3 and 4] with $\tau = 1200$ s, $x = 0.50$, and $c = 1.4$ Pa·s$^{1/2}$ in (a) and $\tau = 1200$ s, $x = 0.53$, and $c = 41$ Pa·s$^{1/2}$ in (b). (c) Fit parameter x, which is constant $x = 0.5 \pm 0.1$, irrespective of the CB content as shown by the dashed line. (d) Fit parameter $\mathcal{G}_0$, which increases as a power law of x_{CB} with an exponent 4.7 ± 0.7.

https://doi.org/10.1021/acs.macromol.2c02068
Macromolecules 2023, 56, 2298−2308

yields a constant effective temperature, $x \simeq 0.5 < 1$ [Figure 8c], that is characteristic of a yield stress fluid,[101] and a reference modulus $\mathcal{G}_0$ that grows as a power law of the CB weight fraction, with an exponent 4.7 [Figure 8d]. First, the latter value is much larger than 1.8, which allows us to rule out a microstructure involving polymer-bridged nanoparticles.[104,105] Second, the exponent 4.7 is consistent with that reported for CB gels in aprotic solvents, e.g., mineral oils, in which the elasticity also originates from a percolated network of CB particles,[24,29] as well as in depletion gels.[106] Similarly, the Brownian parameter c follows a power law of the CB content as shown in Figure S8.

Varying the polymer concentration as well as the CB content, we observe that the gel reference modulus falls onto a master curve when plotted as a function of $(r_c - r)^{\xi} x_{CB}^{\beta}$, as illustrated in Figure 9 with $\xi = 3.8$ and $\beta = 8.2$. This expression

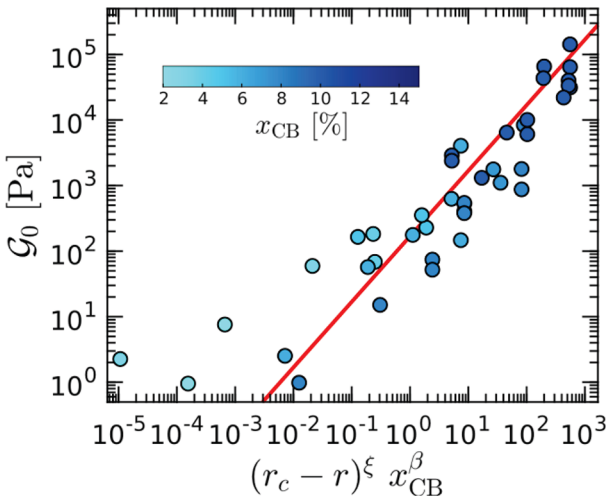

Figure 9. Scaling of the elastic modulus in the colloid-dominated regime. Elastic modulus $\mathcal{G}_0$ vs $(r_c - r)^{\xi} x_{CB}^{\beta}$ for $r < r_c$, where $r_c = 0.037$, $\xi = 3.8 \pm 0.5$, and $\beta = 8.2 \pm 0.6$ (consistent with Figure 4). Color levels code for the CB content ranging between 2% and 10%. The red line shows the best linear fit of the data.

accounts for the scalings displayed in Figure 4a and for the fact that, as $r \to r_c$, the elastic properties vanish, for the CB particles and clusters become isolated in the CMC matrix. Note, as detailed in the Supporting Information, that these exponents are fully consistent with the power-law dependence of $\mathcal{G}_0$ found in Figure 8.

Finally, CMC−CB hydrogels in the colloid-dominated regime (i.e., $r < r_c$) are electrically conductive [Figure 4b]. In Figure 10, we compare their mechanical and electrical properties and observe that the electrical conductivity σ_{CB} conferred upon the sample by the percolated network of CB particles increases as a power law of the reference modulus $\mathcal{G}_0$ with an exponent of about 0.6. Note that a compatible exponent of 0.6 was robustly observed with the same type of CB particles dispersed in mineral oil at various weight fractions in the absence of any dispersant and for various shear histories.[33] This comparison strongly suggests that, for $r < r_c$, CMC only serves to stabilize the CB network in water, without affecting the link between the mechanical and electrical properties, at least for $r \ll r_c$. Yet, one should emphasize that CMC−CB hydrogels display much lower conductivity values ranging between 10^{-4} and 10^{-2} mS/cm, compared to

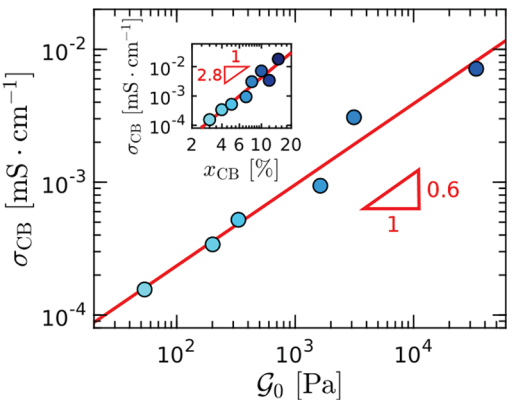

Figure 10. Electrical conductivity of the CB network σ_{CB} vs the elastic modulus G_0. The colors indicate the values of x_{CB} using the same scale as in Figure 9. The red line is the best power-law fit with an exponent 0.6 ± 0.2. Inset: σ_{CB} vs x_{CB}. The red line is the best power-law fit with an exponent 2.8 ± 0.4.

that measured for CB in mineral oil (between 10^{-2} and 2 mS/cm), at similar weight fractions. This discrepancy most likely results from the coating of the CB particles by the CMC, which lowers the conductivity.

DISCUSSION AND CONCLUSION

By performing a fundamental and extensive study of aqueous dispersions of cellulose gum and carbon black soot particles, we have identified the range of polymer and particle contents for which the mixture forms hydrogels. These soft solids show two strikingly different microstructures and mechanical responses depending on the ratio r that quantifies the relative content of polymers and CB particles.

For $r \ll r_c$, i.e., relatively low CMC concentrations, the gel elasticity is governed by the CB particles, which form a space-spanning network. Such a particulate network, which is responsible for the conductive properties of the hydrogel, is decorated and thus stabilized by the CMC. In this regime, the viscoelastic properties of the CMC−CB hydrogel, which are well-described by the SGR model, display weakly aging properties, which might be due to the slow reorganization of the particulate network.

In contrast, for $r \gg r_c$, i.e., relatively high CMC concentrations, the gel elasticity originates from two independent contributions, namely, the entangled CMC matrix on the one hand and the CB particles on the other hand. In this regime, CB particles are dispersed inside the CMC matrix, where they act as cross-linkers through hydrophobic interactions. As a consequence, the sample is not electronically conductive. Moreover, the viscoelastic spectra of these CMC−CB hydrogels are frequency dependent and can be rescaled onto a master curve, which is very-well described by a fractional Kelvin−Voigt model with an exponent $\alpha = 2/3$ that characterizes the high-frequency viscoelastic response.

Interestingly, a similar master curve was reported for CMC−polydispersed silica hydrogels.[107] Although the impact of the CMC concentration was not determined, the scaling factor G_0 was reported to increase as a power law of the silica content with an exponent 3.15 compatible with the value $\zeta = 3.0 \pm 0.5$ reported in Figure 7. This comparison suggests that the nature and specific properties of the suspended nanoparticles, e.g., shape and size, have little or no influence on this exponent, which is mainly controlled by CMC. Moreover, the viscoelastic

https://doi.org/10.1021/acs.macromol.2c02068
Macromolecules 2023, 56, 2298−2308

spectrum of CMC−silica hydrogels show a power law in the high-frequency limit, with an exponent 0.56 that is compatible with the Zimm scaling $\alpha = 2/3$ reported in the present work. Note that this exponent is not universal and depends on the polymer−solvent interaction. For instance, the viscoelastic spectrum of polyacrylamide−silica hydrogels obtained for various contents in silica particles[108] can also be rescaled onto a master curve that shows a high-frequency response that is a power law with an exponent 0.74.

Our results pave the way for the rational design of CMC-based slurries in which CMC is used as a binder, e.g., for lithium-ion batteries,[67,109,110] and more generally for CMC-based hydrogels involving various types of fillers such as graphene oxide, metallic nanoparticles, etc.[111−113] Future work shall include rheo-electric studies of the yielding transition and flow properties of CMC−CB hydrogels, so as to unveil the microscopic scenario underpinning their nonlinear properties.

■ ASSOCIATED CONTENT

Supporting Information

The Supporting Information is available free of charge at https://pubs.acs.org/doi/10.1021/acs.macromol.2c02068.

(i) Dynamic recovery of various CMC−CB hydrogels following flow cessation; (ii) calibration of the conductivity cell; (iii) impact of the CMC concentration on the parameters of the electrical model; (iv) phase diagrams based on the elastic and viscous modulus; (v) scaling of the elastic modulus with the CMC concentration for $r < r_c$; (vi) master curve for the hydrogel viscoelastic spectra for different CMC and CB contents; (vii) dependence on the CB content of the parameter c from the modified SGR model (PDF)

■ AUTHOR INFORMATION

Corresponding Author

Thibaut Divoux − *ENSL, CNRS, Laboratoire de Physique, F-69342 Lyon, France;* orcid.org/0000-0002-6777-5084; Email: Thibaut.Divoux@ens-lyon.fr

Authors

Gauthier Legrand − *ENSL, CNRS, Laboratoire de Physique, F-69342 Lyon, France*

Sébastien Manneville − *ENSL, CNRS, Laboratoire de Physique, F-69342 Lyon, France; Institut Universitaire de France (IUF), F-69342 Lyon, France*

Gareth H. McKinley − *Hatsopoulos Microfluids Laboratory, Department of Mechanical Engineering, MIT, Cambridge, Massachusetts 02139, United States;* orcid.org/0000-0001-8323-2779

Complete contact information is available at: https://pubs.acs.org/10.1021/acs.macromol.2c02068

Notes

The authors declare no competing financial interest.

■ ACKNOWLEDGMENTS

The authors thank R. Backov for suggesting the use of CMC as a dispersant, R. Asmi for preliminary experiments, and C. Bucher and V. Andrieux for insightful discussions on the electrochemical properties of conductive fluids. We also thank G. Baeza for his careful reading of the manuscript and acknowledge fruitful discussions with T. Gibaud, A. Helal, K. Ioannidou, R. J.-M. Pellenq, and M. Peyla.

■ REFERENCES

(1) Samson, R. J.; Mulholland, G. W.; Gentry, J. W. Structural analysis of soot agglomerates. *Langmuir* **1987**, *3*, 272−281.

(2) Spinelli, H. J. Polymeric dispersants in ink jet technology. *Adv. Mater.* **1998**, *10*, 1215−1218.

(3) Phillips, C.; Al-Ahmadi, A.; Potts, S.-J.; Claypole, T.; Deganello, D. The effect of graphite and carbon black ratios on conductive ink performance. *J. Mater. Sci.* **2017**, *52*, 9520−9530.

(4) Ehrburger-Dolle, F.; Hindermann-Bischoff, M.; Livet, F.; Bley, F.; Rochas, C.; Geissler, E. Anisotropic Ultra-Small-Angle X-ray Scattering in Carbon Black Filled Polymers. *Langmuir* **2001**, *17*, 329−334.

(5) Huang, J.-C. Carbon black filled conducting polymers and polymer blends. *Adv. Polym. Technol.* **2002**, *21*, 299−313.

(6) Wen, S.; Chung, D. D. L. Partial replacement of carbon fiber by carbon black in multifunctional cement−matrix composites. *Carbon* **2007**, *45*, 505−513.

(7) Pandolfo, A.; Hollenkamp, A. F. Carbon properties and their role in supercapacitors. *J. Power Sources* **2006**, *157*, 11−27.

(8) Silva, T. A.; Moraes, F. C.; Janegitz, B. C.; Fatibello-Filho, O. Electrochemical biosensors based on nanostructured carbon black: A review. *J. Nanomater.* **2017**, *2017*, 1.

(9) Kour, R.; Arya, S.; Young, S.-J.; Gupta, V.; Bandhoria, P.; Khosla, A. Recent advances in carbon nanomaterials as electrochemical biosensors. *J. Electrochem. Soc.* **2020**, *167*, 037555.

(10) Arduini, F.; Cinti, S.; Mazzaracchio, V.; Scognamiglio, V.; Amine, A.; Moscone, D. Carbon black as an outstanding and affordable nanomaterial for electrochemical (bio) sensor design. *Biosens. Bioelectron.* **2020**, *156*, 112033.

(11) Duduta, M.; Ho, B.; Wood, V. C.; Limthongkul, P.; Brunini, V. E.; Carter, W. C.; Chiang, Y. M. Semi-Solid Lithium Rechargeable Flow Battery. *Adv. Energy Mater.* **2011**, *1*, 511−516.

(12) Li, Z.; Smith, K. C.; Dong, Y.; Baram, N.; Fan, F. Y.; Xie, J.; Limthongkul, P.; Carter, W. C.; Chiang, Y.-M. Aqueous semi-solid flow cell: demonstration and analysis. *Phys. Chem. Chem. Phys.* **2013**, *15*, 15833−15839.

(13) Youssry, M.; Madec, L.; Soudan, P.; Cerbelaud, M.; Guyomard, D.; Lestriez, B. Non-aqueous carbon black suspensions for lithium-based redox flow batteries: rheology and simultaneous rheo-electrical behavior. *Phys. Chem. Chem. Phys.* **2013**, *15*, 14476−14486.

(14) Narayanan, A.; Mugele, F.; Duits, M. H. G. Mechanical History Dependence in Carbon Black Suspensions for Flow Batteries: A Rheo-Impedance Study. *Langmuir* **2017**, *33*, 1629−1638.

(15) Narayanan, T. M.; Zhu, Y. G.; Gençer, E.; McKinley, G. H.; Shao-Horn, Y. Low-cost manganese dioxide semi-solid electrode for flow batteries. *Joule* **2021**, *5*, 2934−2954.

(16) Khodabakhshi, S.; Fulvio, P. F.; Andreoli, E. Carbon black reborn: Structure and chemistry for renewable energy harnessing. *Carbon* **2020**, *162*, 604−649.

(17) Chou, S.-L.; Pan, Y.; Wang, J.-Z.; Liu, H.-K.; Dou, S.-X. Small things make a big difference: binder effects on the performance of Li and Na batteries. *Phys. Chem. Chem. Phys.* **2014**, *16*, 20347−20359.

(18) Parant, H.; Muller, G.; Le Mercier, T.; Tarascon, J. M.; Poulin, P.; Colin, A. Flowing suspensions of carbon black with high electronic conductivity for flow applications: Comparison between carbons black and exhibition of specific aggregation of carbon particles. *Carbon* **2017**, *119*, 10−20.

(19) Youssry, M.; Kamand, F. Z.; Magzoub, M. I.; Nasser, M. S. Aqueous dispersions of carbon black and its hybrid with carbon nanofibers. *RSC Adv.* **2018**, *8*, 32119−32131.

(20) Meslam, M.; Elzatahry, A. A.; Youssry, M. Promising aqueous dispersions of carbon black for semisolid flow battery application. *Colloids Surf. A: Physicochem. Eng. Asp.* **2022**, *648*, 129376.

(21) van der Waarden, M. Stabilization of carbon black dispersion in hydrocarbons. *J. Colloid Sci.* **1950**, *5*, 317−325.

(22) Hartley, P. A.; Parfitt, G. D. Dispersion of powders in liquids. 1. The contribution of the van der Waals force to the cohesiveness of carbon black powders. *Langmuir* **1985**, *1*, 651−657.
(23) Trappe, V.; Pitard, E.; Ramos, L.; Robert, A.; Bissig, H.; Cipelletti, L. Investigation of q-dependent dynamical heterogeneity in a colloidal gel by x-ray photon correlation spectroscopy. *Phys. Rev. E* **2007**, *76*, 051404.
(24) Trappe, V.; Weitz, D. A. Scaling of the viscoelasticity of weakly attractive particles. *Phys. Rev. Lett.* **2000**, *85*, 449−452.
(25) Trappe, V.; Prasad, V.; Cipelletti, L.; Segre, P. N.; Weitz, D. A. Jamming phase diagram for attractive particles. *Nature* **2001**, *411*, 772−775.
(26) Kawaguchi, M.; Okuno, M.; Kato, T. Rheological Properties of Carbon Black Suspensions in a Silicone Oil. *Langmuir* **2001**, *17*, 6041−6044.
(27) Gibaud, T.; Frelat, D.; Manneville, S. Heterogeneous yielding dynamics in a colloidal gel. *Soft Matter* **2010**, *6*, 3482−3488.
(28) Sprakel, J.; Lindström, S.; Kodger, T.; Weitz, D. Stress enhancement in the delayed yielding of colloidal gels. *Phys. Rev. Lett.* **2011**, *106*, 248303.
(29) Grenard, V.; Divoux, T.; Taberlet, N.; Manneville, S. Timescales in creep and yielding of attractive gels. *Soft Matter* **2014**, *10*, 1555−1571.
(30) Gibaud, T.; Perge, C.; Lindström, S. B.; Taberlet, N.; Manneville, S. Multiple yielding processes in a colloidal gel under large amplitude oscillatory stress. *Soft Matter* **2016**, *12*, 1701−1712.
(31) Ovarlez, G.; Tocquer, L.; Bertrand, F.; Coussot, P. Rheopexy and tunable yield stress of carbon black suspensions. *Soft Matter* **2013**, *9*, 5540−5549.
(32) Divoux, T.; Grenard, V.; Manneville, S. Rheological hysteresis in soft glassy materials. *Phys. Rev. Lett.* **2013**, *110*, 018304.
(33) Helal, H.; Divoux, T.; McKinley, G. H. Simultaneous rheo-electric measurements of strongly conductive complex fluids. *Phys. Rev. Applied* **2016**, *6*, 064004.
(34) Li, H. Y.; Chen, H. Z.; Xu, W. J.; Yuan, F.; Wang, J. R.; Wang, M. Polymer-encapsulated hydrophilic carbon black nanoparticles free from aggregation. *Colloid Surf. A: Physicocgem Eng. Aspect* **2005**, *254*, 173−178.
(35) Paredes, J.; Gracia, M.; Martínez-Alonso, A.; Tascón, J. Nanoscale investigation of the structural and chemical changes induced by oxidation on carbon black surfaces: A scanning probe microscopy approach. *J. Colloid Interface Sci.* **2005**, *288*, 190−199.
(36) Liu, T.; Jia, S.; Kowalewski, T.; Matyjaszewski, K.; Casado-Portilla, R.; Belmont, J. Grafting poly (n-butyl acrylate) from a functionalized carbon black surface by atom transfer radical polymerization. *Langmuir* **2003**, *19*, 6342−6345.
(37) Liu, T.; Jia, S.; Kowalewski, T.; Matyjaszewski, K.; Casado-Portilla, R.; Belmont, J. Water-dispersible carbon black nano-composites prepared by surface-initiated atom transfer radical polymerization in protic media. *Macromolecules* **2006**, *39*, 548−556.
(38) Lin, J.-H.; Chen, H.-W.; Wang, K.-T.; Liaw, F.-H. A novel method for grafting polymers on carbon blacks. *J. Mater. Chem.* **1998**, *8*, 2169−2173.
(39) Tsubokawa, N. Functionalization of carbon material by surface grafting of polymers. *Bull. Chem. Soc. Jpn.* **2002**, *75*, 2115−2136.
(40) Yang, Q.; Wang, L.; Xiang, W.; Zhou, J.; Hua Tan, Q. A temperature-responsive carbon black nanoparticle prepared by surface-induced reversible addition−fragmentation chain transfer polymerization. *Polymer* **2007**, *48*, 3444−3451.
(41) Pei, Y.; Travas-Sejdic, J.; Williams, D. E. Water structure change-induced expansion and collapse of zwitterionic polymers surface-grafted onto carbon black. *Aust. J. Chem.* **2014**, *67*, 1706−1709.
(42) Wang, L.; Zhang, L.; Wang, D.; Li, M.; Du, C.; Fu, S. Surface modification of carbon black by thiolene click reaction for improving dispersibility in aqueous phase. *J. Dispers. Sci. Technol.* **2019**, *40*, 152−160.
(43) Tiarks, F.; Landfester, K.; Antonietti, M. Encapsulation of carbon black by miniemulsion polymerization. *Macromol. Chem. Phys.* **2001**, *202*, 51−60.
(44) Casado, R. M.; Lovell, P. A.; Navabpour, P.; Stanford, J. L. Polymer encapsulation of surface-modified carbon blacks using surfactant-free emulsion polymerisation. *Polymer* **2007**, *48*, 2554−2563.
(45) Alves, B. R.; Cooper, W. D. Colloid stabilisation by polyelectrolytes. Dispersions of carbon black in aqueous poly (acrylic acid) solution. *J. Chem. Soc., Faraday Trans. 1* **1981**, *77*, 889−896.
(46) Iijima, M.; Yamazaki, M.; Nomura, Y.; Kamiya, H. Effect of structure of cationic dispersants on stability of carbon black nanoparticles and further processability through layer-by-layer surface modification. *Chem. Eng. Sci.* **2013**, *85*, 30−37.
(47) Hanada, Y.; Masuda, S.; Iijima, M.; Kamiya, H. Analysis of dispersion and aggregation behavior of carbon black particles in aqueous suspension by colloid probe AFM method. *Adv. Powder Technol.* **2013**, *24*, 844−851.
(48) Ogura, T.; Tanoura, M.; Hiraki, A. Behavior of surfactants in the suspension of coal components. *Bull. Chem. Soc. Jpn.* **1993**, *66*, 1633−1639.
(49) Ogura, T.; Tanoura, M.; Tatsuhara, K.; Hiraki, A. The Role of Surfactants in Achieving Highly Loaded Aqueous Suspensions of Organic Particles. *Bull. Chem. Soc. Jpn.* **1994**, *67*, 3143−3149.
(50) Gupta, S. D.; Bhagwat, S. S. Adsorption of surfactants on carbon black-water interface. *J. Dispers. Sci. Technol.* **2005**, *26*, 111−120.
(51) Zhao, Y.; Lu, P.; Li, C.; Fan, X.; Wen, Q.; Zhan, Q.; Shu, X.; Xu, T.; Zeng, G. Adsorption mechanism of sodium dodecyl benzene sulfonate on carbon blacks by adsorption isotherm and zeta potential determinations. *Environ. Technol.* **2013**, *34*, 201−207.
(52) Mizukawa, H.; Kawaguchi, M. Effects of perfluorosulfonic acid adsorption on the stability of carbon black suspensions. *Langmuir* **2009**, *25*, 11984−11987.
(53) Subramanian, S.; Øye, G. Aqueous carbon black dispersions stabilized by sodium lignosulfonates. *Colloid Polym. Sci.* **2021**, *299*, 1223−1236.
(54) Celik, M. Adsorption of ethoxylated sulfonate and nonionic homologs on coal. *J. Colloid Interface Sci.* **1989**, *129*, 428−440.
(55) Bele, M.; Kodre, A.; Arčon, I.; Grdadolnik, J.; Pejovnik, S.; Besenhard, J. Adsorption of cetyltrimethylammonium bromide on carbon black from aqueous solution. *Carbon* **1998**, *36*, 1207−1212.
(56) Porcher, W.; Lestriez, B.; Jouanneau, S.; Guyomard, D. Optimizing the surfactant for the aqueous processing of LiFePO4 composite electrodes. *J. Power Sources* **2010**, *195*, 2835−2843.
(57) Eisermann, C.; Damm, C.; Winzer, B.; Peukert, W. Stabilization of carbon black particles with cetyltrimethylammoniumbromide in aqueous media. *Power Technology* **2014**, *253*, 338−346.
(58) Ridaoui, H.; Jada, A.; Vidal, L.; Donnet, J.-B. Effect of cationic surfactant and block copolymer on carbon black particle surface charge and size. *Colloids Surf. A: Physicochem. Eng. Asp.* **2006**, *278*, 149−159.
(59) Sis, H.; Birinci, M. Effect of nonionic and ionic surfactants on zeta potential and dispersion properties of carbon black powders. *Colloids Surf. A: Physicochem. Eng. Asp.* **2009**, *341*, 60−67.
(60) Lin, Y.; Smith, T. W.; Alexandridis, P. Adsorption of a rake-type siloxane surfactant onto carbon black nanoparticles dispersed in aqueous media. *Langmuir* **2002**, *18*, 6147−6158.
(61) Miano, F.; Bailey, A.; Luckham, P.; Tadros, T. F. Adsorption of nonyl phenol propylene oxide—ethylene oxide surfactants on carbon black and the rheology of the resulting dispersions. *Colloids Surf.* **1992**, *62*, 111−118.
(62) Yasin, S.; Luckham, P. Investigating the effectiveness of PEO/PPO based copolymers as dispersing agents for graphitic carbon black aqueous dispersions. *Colloids Surf. A: Physicochem. Eng. Asp.* **2012**, *404*, 25−35.
(63) N'gouamba, E.; Goyon, J.; Tocquer, L.; Oerther, T.; Coussot, P. Yielding, thixotropy, and strain stiffening of aqueous carbon black suspensions. *J. Rheol.* **2020**, *64*, 955−968.

https://doi.org/10.1021/acs.macromol.2c02068
Macromolecules 2023, 56, 2298−2308

(64) Guerfi, A.; Kaneko, M.; Petitclerc, M.; Mori, M.; Zaghib, K. LiFePO4 water-soluble binder electrode for Li-ion batteries. *J. Power Sources* **2007**, *163*, 1047−1052.
(65) Lee, J.-H.; Kim, J.-S.; Kim, Y. C.; Zang, D. S.; Choi, Y.-M.; Park, W. I.; Paik, U. Effect of carboxymethyl cellulose on aqueous processing of LiFePO4 cathodes and their electrochemical performance. *Electrochem. Solid-State Lett.* **2008**, *11*, A175.
(66) Porcher, W.; Lestriez, B.; Jouanneau, S.; Guyomard, D. Design of aqueous processed thick LiFePO4 composite electrodes for high-energy lithium battery. *J. Electrochem. Soc.* **2009**, *156*, A133.
(67) García, A.; Culebras, M.; Collins, M. N.; Leahy, J. J. Stability and rheological study of sodium carboxymethyl cellulose and alginate suspensions as binders for lithium ion batteries. *J. Appl. Polym. Sci.* **2018**, *135*, 46217.
(68) Barrie, C.; Griffiths, P.; Abbott, R.; Grillo, I.; Kudryashov, E.; Smyth, C. Rheology of aqueous carbon black dispersions. *J. Colloid Interface Sci.* **2004**, *272*, 210−217.
(69) Aoki, Y.; Hatano, A.; Watanabe, H. Rheology of carbon black suspensions. I. Three types of viscoelastic behavior. *Rheol. Acta* **2003**, *42*, 209−216.
(70) Rahman, M. S.; Hasan, M. S.; Nitai, A. S.; Nam, S.; Karmakar, A. K.; Ahsan, M. S.; Shiddiky, M. J.; Ahmed, M. B. Recent developments of carboxymethyl cellulose. *Polymers* **2021**, *13*, 1345.
(71) Jiang, L.; Li, Y.; Zhang, L.; Wang, X. Preparation and characterization of a novel composite containing carboxymethyl cellulose used for bone repair. *Mater. Sci. Eng., C* **2009**, *29*, 193−198.
(72) Kulicke, W.-M.; Kull, A. H.; Kull, W.; Thielking, H.; Engelhardt, J.; Pannek, J.-B. Characterization of aqueous carboxymethylcellulose solutions in terms of their molecular structure and its influence on rheological behaviour. *Polymer* **1996**, *37*, 2723−2731.
(73) Clasen, C.; Kulicke, W.-M. Determination of viscoelastic and rheo-optical material functions of water-soluble cellulose derivatives. *Prog. Polym. Sci.* **2001**, *26*, 1839−1919.
(74) Ghannam, M. T.; Esmail, M. N. Rheological properties of carboxymethyl cellulose. *J. Appl. Polym. Sci.* **1997**, *64*, 289−301.
(75) Benchabane, A.; Bekkour, K. Rheological properties of carboxymethyl cellulose (CMC) solutions. *Colloid Polym. Sci.* **2008**, *286*, 1173−1180.
(76) Elliott, J. H.; Ganz, A. J. Modification of food characteristics with cellulose hydrocolloids I: Rheological characterization of an organoleptic property (unctuousness). *J. Texture Stud.* **1971**, *2*, 220−229.
(77) Barba, C.; Montané, D.; Farriol, X.; Desbrières, J.; Rinaudo, M. Synthesis and characterization of carboxymethylcelluloses from non-wood pulps II. Rheological behavior of CMC in aqueous solution. *Cellulose* **2002**, *9*, 327−335.
(78) Medronho, B.; Romano, A.; Miguel, M. G.; Stigsson, L.; Lindman, B. Rationalizing cellulose (in) solubility: reviewing basic physicochemical aspects and role of hydrophobic interactions. *Cellulose* **2012**, *19*, 581−587.
(79) Glasser, W. G.; Atalla, R. H.; Blackwell, J.; Malcolm Brown, R.; Burchard, W.; French, A. D.; Klemm, D. O.; Nishiyama, Y. About the structure of cellulose: debating the Lindman hypothesis. *Cellulose* **2012**, *19*, 589−598.
(80) Lopez, C. G.; Colby, R. H.; Cabral, J. T. Electrostatic and hydrophobic interactions in NaCMC aqueous solutions: Effect of degree of substitution. *Macromolecules* **2018**, *51*, 3165−3175.
(81) Lopez, C. G.; Richtering, W. Oscillatory rheology of carboxymethyl cellulose gels: Influence of concentration and pH. *Carbohydr. Polym.* **2021**, *267*, 118117.
(82) Le Ouay, B.; Lau-Truong, S.; Flahaut, E.; Brayner, R.; Aubard, J.; Coradin, T.; Laberty-Robert, C. DWCNT-doped silica gel exhibiting both ionic and electronic conductivities. *J. Phys. Chem. C* **2012**, *116*, 11306−11314.
(83) Youssry, M.; Guyomard, D.; Lestriez, B. Suspensions of carbon nanofibers in organic medium: Rheo-electrical properties. *Phys. Chem. Chem. Phys.* **2015**, *17*, 32316−32327.
(84) Cole, K. S. Electric impedance of suspensions of spheres. *J. Gen. Physiol.* **1928**, *12*, 29.
(85) Macdonald, J. R.; Barsoukov, E. *Impedance spectroscopy: theory, experiment, and applications*; John Wiley & Sons, 2018.
(86) Lasia, A. The origin of the constant phase element. *J. Phys. Chem. Lett.* **2022**, *13*, 580−589.
(87) Baeza, G. P.; Oberdisse, J.; Alegria, A.; Saalwächter, K.; Couty, M.; Genix, A.-C. Depercolation of aggregates upon polymer grafting in simplified industrial nanocomposites studied with dielectric spectroscopy. *Polymer* **2015**, *73*, 131−138.
(88) Jaishankar, A.; McKinley, G. H. Power-law rheology in the bulk and at the interface: quasi-properties and fractional constitutive equations. *Proc. R. Soc. A: Math. Phys. Eng. Sci.* **2013**, *469*, 20120284.
(89) Bonfanti, A.; Kaplan, J. L.; Charras, G.; Kabla, A. Fractional viscoelastic models for power-law materials. *Soft Matter* **2020**, *16*, 6002−6020.
(90) Scott-Blair, G. W. S.; Burnett, J. On the creep, recovery, relaxation and elastic "memory" of some renneted milk gels. *Br. J. Appl. Phys.* **1959**, *10*, 15.
(91) Zimm, B. H. Dynamics of polymer molecules in dilute solution: viscoelasticity, flow birefringence and dielectric loss. *J. Chem. Phys.* **1956**, *24*, 269−278.
(92) Bagley, R. L.; Torvik, P. A theoretical basis for the application of fractional calculus to viscoelasticity. *J. Rheol.* **1983**, *27*, 201−210.
(93) Colby, R. H.; Rubinstein, M.; Viovy, J. L. Chain entanglement in polymer melts and solutions. *Macromolecules* **1992**, *25*, 996−998.
(94) Behra, J. S.; Mattsson, J.; Cayre, O. J.; Robles, E. S.; Tang, H.; Hunter, T. N. Characterization of sodium carboxymethyl cellulose aqueous solutions to support complex product formulation: A rheology and light scattering study. *ACS Appl. Mater. Interfaces.* **2019**, *1*, 344−358.
(95) Mason, T. G.; Weitz, D. A. Optical measurements of frequency-dependent linear viscoelastic moduli of complex fluids. *Phys. Rev. Lett.* **1995**, *74*, 1250.
(96) Purnomo, E. H.; Van Den Ende, D.; Vanapalli, S. A.; Mugele, F. Glass transition and aging in dense suspensions of thermosensitive microgel particles. *Phys. Rev. Lett.* **2008**, *101*, 238301.
(97) Aime, S.; Cipelletti, L.; Ramos, L. Power law viscoelasticity of a fractal colloidal gel. *J. Rheol.* **2018**, *62*, 1429−1441.
(98) Keshavarz, B.; Rodrigues, D. G.; Champenois, J.-B.; Frith, M. G.; Ilavsky, J.; Geri, M.; Divoux, T.; McKinley, G. H.; Poulesquen, A. Time−connectivity superposition and the gel/glass duality of weak colloidal gels. *Proc. Natl. Acad. Sci. U.S.A.* **2021**, *118*, No. e2022339118.
(99) Sollich, P.; Lequeux, F.; Hébraud, P.; Cates, M. E. Rheology of soft glassy materials. *Phys. Rev. Lett.* **1997**, *78*, 2020.
(100) Sollich, P. Rheological constitutive equation for a model of soft glassy materials. *Phys. Rev. E* **1998**, *58*, 738−759.
(101) Fielding, S. M.; Sollich, P.; Cates, M. E. Aging and rheology in soft materials. *J. Rheol.* **2000**, *44*, 323−369.
(102) Purnomo, E.; Van Den Ende, D.; Mellema, J.; Mugele, F. Linear viscoelastic properties of aging suspensions. *Europhys. Lett.* **2006**, *76*, 74.
(103) Mason, T.; Weitz, D. Linear viscoelasticity of colloidal hard sphere suspensions near the glass transition. *Phys. Rev. Lett.* **1995**, *75*, 2770.
(104) Surve, M.; Pryamitsyn, V.; Ganesan, V. Universality in structure and elasticity of polymer-nanoparticle gels. *Phys. Rev. Lett.* **2006**, *96*, 177805.
(105) Surve, M.; Pryamitsyn, V.; Ganesan, V. Polymer-bridged gels of nanoparticles in solutions of adsorbing polymers. *J. Chem. Phys.* **2006**, *125*, 064903.
(106) Prasad, V.; Trappe, V.; Dinsmore, A. D.; Segre, P. N.; Cipelletti, L.; Weitz, D. A. Universal features of the fluid to solid transition for attractive colloidal particles. *Faraday Discuss.* **2003**, *123*, 1−12.
(107) Pashkovski, E. E.; Masters, J. G.; Mehreteab, A. Viscoelastic scaling of colloidal gels in polymer solutions. *Langmuir* **2003**, *19*, 3589−3595.

https://doi.org/10.1021/acs.macromol.2c02068
Macromolecules 2023, 56, 2298−2308

(108) Adibnia, V.; Hill, R. J. Viscoelasticity of near-critical silica-polyacrylamide hydrogel nanocomposites. *Polymer* **2017**, *112*, 457−465.
(109) Lee, J.-H.; Paik, U.; Hackley, V. A.; Choi, Y.-M. Effect of carboxymethyl cellulose on aqueous processing of natural graphite negative electrodes and their electrochemical performance for lithium batteries. *J. Electrochem. Soc.* **2005**, *152*, A1763.
(110) Dahbi, M.; Nakano, T.; Yabuuchi, N.; Ishikawa, T.; Kubota, K.; Fukunishi, M.; Shibahara, S.; Son, J.-Y.; Cui, Y.-T.; Oji, H.; Komaba, S. Sodium carboxymethyl cellulose as a potential binder for hard-carbon negative electrodes in sodium-ion batteries. *Electrochem. commun.* **2014**, *44*, 66−69.
(111) Bozaci, E.; Akar, E.; Ozdogan, E.; Demir, A.; Altinisik, A.; Seki, Y. Application of carboxymethylcellulose hydrogel based silver nanocomposites on cotton fabrics for antibacterial property. *Carbohydr. Polym.* **2015**, *134*, 128−135.
(112) Ali, N. H.; Amin, M. C. I. M.; Ng, S.-F. Sodium carboxymethyl cellulose hydrogels containing reduced graphene oxide (rGO) as a functional antibiofilm wound dressing. *J. Biomater. Sci. Polym. Ed.* **2019**, *30*, 629−645.
(113) Saladino, M. L.; Markowska, M.; Carmone, C.; Cancemi, P.; Alduina, R.; Presentato, A.; Scaffaro, R.; Biały, D.; Hasiak, M.; Hreniak, D.; Wawrzyńska, M. Graphene oxide carboxymethylcellulose nanocomposite for dressing materials. *Materials* **2020**, *13*, 1980.

https://doi.org/10.1021/acs.macromol.2c02068
Macromolecules 2023, 56, 2298−2308